

# Fe/C Nanocapsule-Decorated Fe<sub>2</sub>B/C Nanocapsule Hybrids with Improved Gigahertz Electromagnetic Absorption Properties

Xianguo Liu, Mingji Zhang, Siu Wing Or, and Siu Lau Ho

Department of Electrical Engineering, The Hong Kong Polytechnic University, Hung Hom, Kowloon, Hong Kong

**We report an obvious improvement in gigahertz electromagnetic absorption properties in novel core/shell-structured magnetic/dielectric nanocapsule-decorated nanocapsule hybrids, featuring Fe/C nanocapsules of ~4 nm mean diameter decorated on the surfaces of Fe<sub>2</sub>B/C nanocapsules of ~50 nm mean diameter (denoted as Fe/C@Fe<sub>2</sub>B/C hybrids), as a result of the simultaneously enhanced dielectric and magnetic losses by an increased interfacial polarization at the Fe/C and Fe<sub>2</sub>B/C heterogeneous interfaces and an additional tip effect by the decoration of small Fe/C nanocapsules. The phase, morphology, microstructure, and magnetization of the Fe/C@Fe<sub>2</sub>B/C hybrids are investigated using various methods, and their electromagnetic absorption properties are evaluated in paraffin-bonded composites with 50 wt.% hybrids over the 2–18 GHz range. The results indicate a giant reflection loss (*RL*) of –49.5 dB at 10.5 GHz and a broad effective absorption bandwidth (for *RL* < –10 dB) of 8 GHz at a thin composite thickness of 2.1 mm. An extremely broad coverage of effective absorption bandwidth from 2.5 to 18 GHz is obtained at a very wide composite thickness range of 1–6 mm. The present study provides a new prospective for realizing high-performance EM absorbers at gigahertz frequencies.**

**Index Terms**—Core/shell structure, decoration, electromagnetic absorption properties, hybrid, nanocapsules.

## I. INTRODUCTION

**T**H rapid development and application of high-speed and high-frequency electronic and information technologies in the gigahertz (GHz) frequency range have greatly increased the impact of electromagnetic (EM) radiation on our society [1]. Accordingly, much research effort has been devoted to developing high-performance EM absorbers having strong absorption, broad absorption bandwidth, thin thickness, wide thickness range, and low density in the GHz range over the past decade [2]–[8]. EM absorbers are typically designed to minimize reflection so as to maximally introduce and absorb EM energy through an EM impedance match at frequencies of interest. They are generally characterized by reflection loss (*RL*) in that an excess in *RL* of –10 and –20 dB, corresponding to 90 and 99% absorption, is regarded as efficient for general and higher-end uses, respectively [2]–[7].

Core/shell-structured magnetic/dielectric nanocapsules that are formed by a magnetic nanoparticle core and a dielectric thin shell have attracted great attention as new generation EM absorbers because of their simple structure, easy preparation, strong synergy between dielectric and magnetic losses, etc. [2]–[9]. The high-magnetic-loss and low-cost natures of soft metallic magnetic nanomaterials have made them popular for use as magnetic nanoparticle core. The low density, good dielectric properties, high stability, cost-effectiveness, etc. of carbon have made it a stand-out dielectric thin shell candidate for matching while protecting the soft metallic magnetic nanoparticle core from oxidation and/or corrosion [7]–[11].

Onion-like carbon (or curved graphite) has been studied recently as dielectric thin shell in various core/shell-structured magnetic/dielectric nanocapsules, including Ni/C, Fe/C, Co/C, FeNi/C, and CoNi/C nanocapsules [3], [9]–[15]. The observed

good EM absorption properties have been ascribed to the steady permittivity and permeability, the good EM impedance match, the high Snoek's limitation, etc. In fact, there exist many lattice defects (e.g., carbon-layer breakage, blending in homocentric sphere layers, etc.) and structural defects (e.g., interstitial atoms, stacking faults, dislocation of carbon layers, etc.) in onion-like carbon shell as a result of the rapid cooling and the resulting curved shape. These defects act as active sites for dipolar polarization [16]. However, the mutual exclusion in the dielectric and magnetic losses usually leads to the weakening of one quantity in an attempt to enhance another quantity by increasing its component fraction, thereby limiting the resulting *RL* values [15]. Inspired by dumbbell-like Fe<sub>3</sub>O<sub>4</sub>–Au nanoparticles, an innovative use of a special nanostructure is capable of inducing interfacial polarization and tip effect for improving EM absorption properties [17].

In this paper, we present a new approach to improve the GHz EM absorption properties of nanocapsules by decorating small nanocapsules on the surfaces of large nanocapsules to form novel nanocapsule-decorated nanocapsule hybrids. As a demonstration, Fe/C nanocapsules of ~4 nm mean diameter are decorated on the surfaces of Fe<sub>2</sub>B/C nanocapsules of ~50 nm mean diameter to form Fe/C@Fe<sub>2</sub>B/C hybrids using an arc-discharge process. The decoration is aimed to increase the interfacial polarization by creating more heterogeneous interfaces between the Fe/C and Fe<sub>2</sub>B/C nanocapsules. It is also aimed to introduce a tip effect by decorating small Fe/C nanocapsules on the large Fe<sub>2</sub>B/C nanocapsules. As a result, the dielectric and magnetic losses of the Fe/C@Fe<sub>2</sub>B/C hybrids are enhanced, and so do the *RL* values and the absorption bandwidths, in the GHz range and at a thinner absorber thickness and a wider absorber thickness range compared to the mixture of Fe/C and Fe<sub>2</sub>B/C nanocapsules.

## II. PREPARATION AND EVALUATIONS

The Fe/C@Fe<sub>2</sub>B/C hybrids were prepared by a controlled arc-discharge process. Powders of Fe and B of 99.9% purity

Manuscript received June 6, 2018; Accepted August 13, 2018  
Corresponding author: S. W. Or (e-mail: eeswor@polyu.edu.hk).

Color versions of one or more of the figures in this paper are available online at <http://ieeexplore.ieee.org>.

Digital Object Identifier (inserted by IEEE).

and with an average size of 10  $\mu\text{m}$  were properly mixed for the preparation of a target. The composition of the target was designed to be  $\text{Fe}_5\text{B}_{95}$  (at%) by considering the difficulty in evaporating B. The  $\text{Fe}_5\text{B}_{95}$  target was attached to a water-cooled graphite crucible as the anode for rapid cooling, while a carbon needle of 5 mm diameter was used as the cathode. After evacuating the arc-discharge chamber to 7 mPa, Ar as a reactant gas and  $\text{H}_2$  as a source of hydrogen plasma were introduced into the chamber to give pressures of 16 and 4 kPa, respectively. Liquid ethanol of 40 ml was injected into the chamber as the carbon source. The arc was ignited and an arc-discharge current of 40 A was applied for 0.5 h. After being passivated in air for 24 h, the product deposited on the graphite crucible was collected. For comparison purpose, the product deposited on the chamber wall was also collected. The details of these two products are discussed in Sec. III.

The phase analysis of the products was performed by an X-ray diffractometer (XRD, Bruker D8 Advance) with monochromatic  $\text{Cu-K}\alpha$  radiation ( $\lambda=1.54 \text{ \AA}$ ). The morphology and microstructure were evaluated by a high-resolution transmission electron microscope (HRTEM, JEOL 2010F) at an emission voltage of 200 kV. The magnetization–magnetic field ( $M$ – $H$ ) curve was obtained using a vibrating sample magnetometer (VSM, Lake Shore 7410) at room temperature. To enable measurements of the EM absorption properties, 50 wt.% of products was ultrasonically mixed with 50 wt.% of EM transparent liquid paraffin and hexane. The mixture was pressed into toroidal composites with an outer diameter of 7.00 mm, an inner diameter of 3.04 mm, and an initial thickness of 6.00 mm after the evaporation of hexane. The scattering ( $S$ -) parameters of the composites were measured at different thicknesses ( $d$ ) by a transmission/reflection coaxial line method in the 2–18 GHz frequency ( $f$ ) range using a computer-controlled network analyzer (Keysight PNA-X N5244A) with short, open, load, and thru calibrations. The complex relative permittivity ( $\epsilon_r = \epsilon_r' - j\epsilon_r''$ ) and complex relative permeability ( $\mu_r = \mu_r' - j\mu_r''$ ) spectra at various  $d$  were determined by a materials measurement software suite (Keysight N1500A) preinstalled in a computer. The reflection loss ( $RL$ ) spectra at various  $d$  were deduced from the determined  $\epsilon_r$  and  $\mu_r$  spectra using [10]:

$$RL = 20 \log |(Z_{\text{in}} - 1)/(Z_{\text{in}} + 1)| \quad (1)$$

where  $Z_{\text{in}} = (\mu_r/\epsilon_r)^{1/2} \tanh[j(2\pi f d/c)(\mu_r \epsilon_r)^{1/2}]$  is the normalized input impedance of the composite,  $j$  is the unit imaginary number, and  $c=3 \times 10^8$  m/s is the velocity of light.

### III. RESULTS AND DISCUSSION

Fig. 1(a) shows the XRD pattern of the product deposited on the graphite crucible. The two small diffraction peaks at  $44.7^\circ$  and  $65.0^\circ$  (marked by black symbol) are indexed as a Fe crystal with a body-centered cubic (bcc) phase in accordance with JCPDS No. 06-0696. Other diffraction peaks (plotted with red line) are confirmed as a  $\text{Fe}_2\text{B}$  crystal with a tetragonal phase in reference to JCPDS No. 36-1332. The formation of the tetragonal phase can be attributed to the collision of Fe and B atoms during evaporation from the molten pool of the anode. Apart from the  $\text{Fe}_2\text{B}$  binary compound, no other intermetallic compounds are observed in the Fe–B binary system. It is noted that  $\text{Fe}_2\text{B}$  is a high-temperature phase stabilizing at 1223–1373

K [18]. The reason why this high-temperature phase is present at room temperature can be explained by the higher surface energy and non-equilibrium formation process of the nanoparticles with metastable phases [19]. Fig. 1(b) plots the magnetization–magnetic field ( $M$ – $H$ ) curve of the product in Fig. 1(a). The small saturation magnetization ( $M_S$ ) of 121 emu/g and coercivity ( $H_C$ ) of 32 Oe indicate a good soft magnetic material. The higher  $M_S$  value than the bulk  $\text{Fe}_2\text{B}$  of 102 emu/g, but lower than the nanocrystalline Fe of 210 emu/g, elucidates a sufficient contribution of the Fe phase to the  $\text{Fe}_2\text{B}$  phase [20].

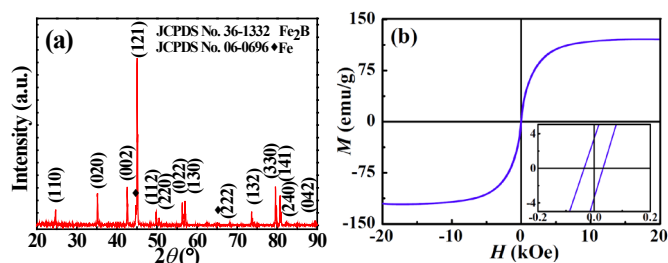


Fig. 1. (a) XRD pattern and (b)  $M$ – $H$  curve of the product deposited on graphite crucible. The inset in (b) shows the enlarged portion at low  $H$  levels.

Figs. 2(a) and 2(b) show the TEM images of the products deposited on the chamber wall and the graphite crucible, respectively. Fig. 2(a) gives a typical form of core/shell-structured nanocapsules with some degrees of irregularity in spherical shape [8]–[15]. The observation agrees with those prepared by traditional arc-discharge process [2], [15]. The overall diameter of the nanocapsules varies from 10 to 80 nm. An agglomeration of the nanocapsules of various sizes is seen, leading to the formation of the mixture of Fe/C and  $\text{Fe}_2\text{B}/\text{C}$  nanocapsules rather than the desired  $\text{Fe}/\text{C}@ \text{Fe}_2\text{B}/\text{C}$  hybrids. By contrast, Fig. 2(b) exhibits a clear decoration of small nanocapsules of  $\sim 4$  nm mean diameter on the surfaces of large nanocapsules of  $\sim 50$  nm mean diameter. Those are the proposed  $\text{Fe}/\text{C}@ \text{Fe}_2\text{B}/\text{C}$  hybrids.

In order to give an insight into the detailed microstructure of the  $\text{Fe}/\text{C}@ \text{Fe}_2\text{B}/\text{C}$  hybrids in Fig. 2(b), the HRTEM images of a large nanocapsule body and a small nanocapsule decoration are illustrated in Figs. 2(c) and 2(d), respectively. Both the large nanocapsule body and the small nanocapsule decoration possess a core/shell structure with the same lattice fringe spacing of 0.34 nm for the shells. This corresponds to the (002) characteristic lattice plane of graphite. Moreover, the different lattice plane spacings of 0.201 nm in the [121] direction in Fig. 2(c) and 0.204 nm in the [110] direction in Fig. 2(d) indicate the  $\text{Fe}_2\text{B}$  and Fe cores, respectively. Thus, the large nanocapsule body and the small nanocapsule decoration in Fig. 2(b) are the  $\text{Fe}_2\text{B}/\text{C}$  nanocapsules in Fig. 2(c) and the Fe/C nanocapsules in Fig. 2(d), respectively. The difference in size can be attributed to the difference in formation mechanism of the two different nanocapsules [19].

In high-temperature plasma, Fe atoms take the priority to evaporate and to bump up with B atoms for the formation of the  $\text{Fe}_2\text{B}$  phase, which is further grown in the plasma zone to form the large  $\text{Fe}_2\text{B}/\text{C}$  nanocapsules. While the excessive Fe atoms are swept out of the plasma zone by the arc pressure, the excessive Fe atoms are rapidly cooled to form the small Fe/C nanocapsules because of the small distance between the

plasma zone and the graphite crucible. As confirmed by Figs. 2(b)–2(d), Fe/C@Fe<sub>2</sub>B/C hybrids are formed. This structural feature can effectively increase the interfacial polarization and give rise to the tip effect to be discussed in Figs. 3 and 4.

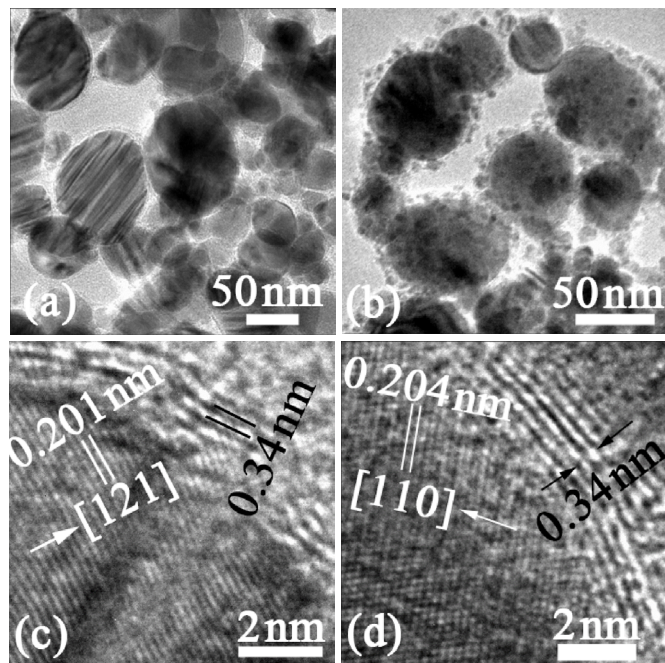


Fig. 2. TEM images of the products deposited on (a) chamber wall and (b) graphite crucible. HRTEM images of (c) a single Fe<sub>2</sub>B/C nanocapsule and (d) a single Fe/C nanocapsule in (b).

In order to study the EM absorption properties of the Fe/C@Fe<sub>2</sub>B/C hybrids in Fig. 2(b), the complex relative permittivity ( $\epsilon_r = \epsilon_r' - j\epsilon_r''$ ) and complex relative permeability ( $\mu_r = \mu_r' - j\mu_r''$ ) spectra of the Fe/C@Fe<sub>2</sub>B/C hybrid composites are investigated and shown in Figs. 3(a) and 3(b), respectively. The Fe/C and Fe<sub>2</sub>B/C mixture in Fig. 2(a) is also investigated in the Fe/C+Fe<sub>2</sub>B/C mixture composites for comparison. For both  $\epsilon_r$  and  $\mu_r$ , the real part represents the storage capability of electric and magnetic energies, while the imaginary part stands for the loss capability of electric and magnetic energies, respectively [10]. In Fig. 3(a),  $\epsilon_r'$  and  $\epsilon_r''$  of the hybrid composites remain almost constant over the whole 2–18 GHz range with only a slight fluctuation in  $\epsilon_r'$  and  $\epsilon_r''$  of  $\sim 6.5$  and  $\sim 2.8$ , respectively. For the mixture composites,  $\epsilon_r'$  and  $\epsilon_r''$  exhibit decreasing trends with increasing  $f$  from 2 to 18 GHz because of the increased lagging in dipolar polarization response with respect to the electric field change at higher frequencies [3]. In Fig. 3(b),  $\mu_r'$  of the hybrid composites decreases from 2.68 to 1.54 in the 2–18 GHz range, while  $\mu_r''$  is almost constant at  $\sim 0.6$ , except for the two small peaks at 3.5 and 13.5 GHz. The mixture composites have similar trends of  $\mu_r'$  and  $\mu_r''$  in that  $\mu_r'$  decreases from 0.9 to 0.8, while  $\mu_r''$  contains two small peaks at 4 and 9 GHz. For both hybrid and mixture composites, the 1<sup>st</sup> peak at 3.5 and 4 GHz can be attributed to Kittel natural resonance [6], while the 2<sup>nd</sup> peak at 13.5 and 9 GHz can be ascribed by Aharoni exchange resonance. The exchange resonance theory developed by Aharoni is commonly adopted to explain multi-resonance behavior of small magnetic particles [6], and the exchange resonance frequency is inversely proportional to particle size. Thus, the exchange resonance in the hybrid composites at 13.5

GHz can be related to the small nanocapsules. The increase of  $\mu_r$  in the hybrid composites can be explained by the enhanced magnetic dipole interaction in the Fe/C@Fe<sub>2</sub>B/C hybrids, which are closer in distance than the mixture of Fe/C and Fe<sub>2</sub>B/C nanocapsules in the mixture composites [15].

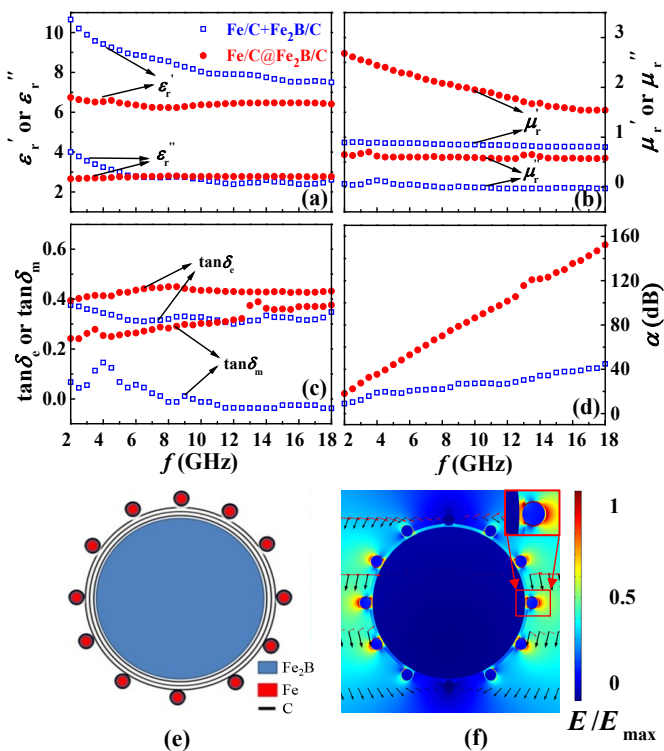


Fig. 3. Spectra of (a)  $\epsilon_r'$  and  $\epsilon_r''$ , (b)  $\mu_r'$  and  $\mu_r''$ , (c)  $\tan \delta_e$  and  $\tan \delta_m$ , (d)  $\alpha$  for Fe/C@Fe<sub>2</sub>B/C hybrid composites and Fe/C+Fe<sub>2</sub>B/C mixture composites. (e) Finite-element model and (f) normalized electric field distribution at 10 GHz for a single Fe/C@Fe<sub>2</sub>B/C hybrid.

Fig. 3(c) shows the dielectric loss factor ( $\tan \delta_e = \epsilon_r''/\epsilon_r'$ ) and magnetic loss factor ( $\tan \delta_m = \mu_r''/\mu_r'$ ) spectra of the hybrid and mixture composites. In practice,  $\tan \delta_e$  and  $\tan \delta_m$  are mutually exclusive and are difficult to be enhanced at the same time in single-component materials.  $\tan \delta_e$  and  $\tan \delta_m$  of the hybrid composites are both higher than the mixture composites in the whole 2–18 GHz range. This implies the existence of a more effective EM absorption in the hybrid composites. Fig. 3(d) shows the attenuation constant ( $\alpha$ ) spectra of the hybrid and mixture composites.  $\alpha$  describes the attenuation properties of a material and is determined by the measured  $\epsilon_r$  and  $\mu_r$  at a given frequency [10]. It is seen that the hybrid composites possess much higher attenuation ability than the mixture composites.

To further investigate the underlying mechanism for the improvement in the GHz EM absorption properties in the hybrid composites, a numerical simulation was performed using COMSOL Multiphysics finite-element analysis. Fig. 3(e) shows the finite-element model composed of twelve 4 nm Fe/C nanocapsules decorated on the surface of a 50 nm Fe<sub>2</sub>B/C nanocapsule. By choosing the conductivity of graphitic shell to be 3 S/m, the simulated dielectric resonance frequencies can be adjusted to match with our experimental results in Fig. 3(a) [3] [8]. Fig. 3(f) shows a normalized electric field distribution in various incident directions at 10 GHz. It is seen that the improvement in the GHz EM

absorption properties is not only due to the interfacial polarization of the Fe/C and Fe<sub>2</sub>B/C heterogeneous interfaces, but also due to the tip effect of the Fe/C nanocapsule decoration as highlighted in the inset of Fig. 3(f) [12].

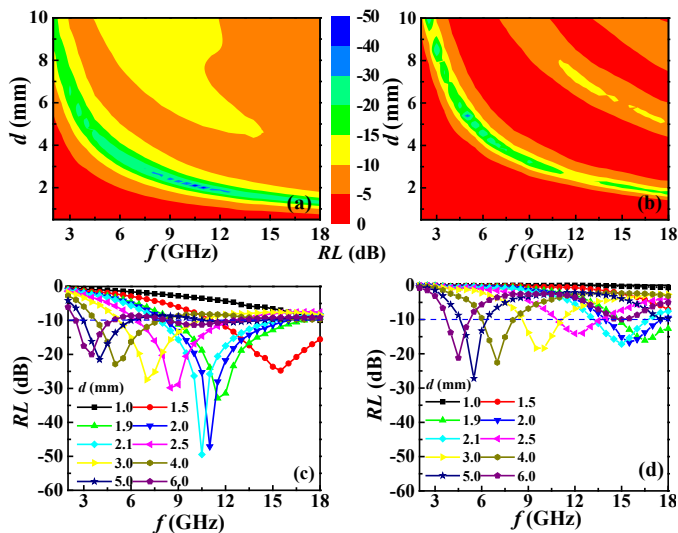


Fig. 4. 2D-contour plots of  $f$  and  $d$  dependences on  $RL$  for (a) hybrid and (b) mixture composites.  $f$  dependence of  $RL$  at various  $d$  for (c) hybrid and (d) mixture composites.

Table I. Summary of some important EM absorption properties of some related previous works at the largest reflection loss.

Nanomaterials	$RL$ (dB)	$f$ (GHz)	$d$ (mm)	$BW_{\text{eff}}$ (GHz)
Present Work	-49.5	10.5	2.1	8 (7.7–15.7)
Sandwich-type graphene/Fe <sub>3</sub> O <sub>4</sub> /carbon microtube [1]	-48	7.8	3	0.5 (6.8–7.3)
Carbon-coated FeSn <sub>2</sub> /Sn nanocomposites [2]	-28	11.8	3.3	7.7 (7.5–15.2)
Graphene foam-supported Ni nanoparticles [4]	-43	7.6	5	4.9 (6.2–11.1)
CoFe <sub>2</sub> O <sub>4</sub> /nitrogen-doped ordered mesoporous carbon composites [5]	-34	8	2.5	2.8 (7.2–10)
BaFe <sub>12</sub> O <sub>19</sub> /Ni <sub>0.5</sub> Zn <sub>0.5</sub> Fe <sub>2</sub> O <sub>4</sub> microfibers [7]	-42.5	10.3	4	11.2 (6.8–18)
Ethylene-vinyl acetate powders and polycrystalline Fe fibers [11]	-42	15.3	2	6.7 (11.3–18)

Figs. 4(a) and 4(b) show the 2D-contour plots of frequency ( $f$ ) and thickness ( $d$ ) dependences on reflection loss ( $RL$ ) for the hybrid and mixture composites, respectively. The  $RL$  peak frequency, namely matching frequency, of both composites shifts to the lower  $f$  side with increasing  $d$ , corresponding well to the model proposed by Naito and Suetake [22]. The correlation between  $RL$  and  $f$  at some selected  $d$  is plotted in Figs. 4(c) and 4(d) for the hybrid and mixture composites, respectively. For the hybrid composites in Fig. 4(c), the lowest  $RL$  value is as small as  $-49.5$  dB at 10.5 GHz for a thin  $d$  of 2.1 mm, and the corresponding effective absorption bandwidth ( $BW_{\text{eff}}$ ) for  $RL < -10$  dB is as broad as 8 GHz (7.7–15.7 GHz). When  $d$  is reduced to 2 and 1.9 mm, the hybrid composites have an impressively broad  $BW_{\text{eff}}$  of 7.5 GHz; that is, from 8.5 to 16 GHz for  $d=2$  mm and from 9 to 16.5 GHz for  $d=1.9$  mm. When  $d$  is as thin as 1.5 mm, a sufficiently broad  $BW_{\text{eff}}$  of 6.5 GHz (11.5–18 GHz) can still be preserved. In contrast, the mixture composites only have the lowest  $RL$  value of  $-27.2$  dB

at 5.5 GHz for a much thicker  $d$  of 5.0 mm. When  $d$  is 2 mm,  $BW_{\text{eff}}$  is as narrow as 3.5 GHz (14–17.5 GHz), which is only  $\sim 47\%$  of the hybrid composites at the same  $d$ . In general, the hybrid composites have an extremely broad coverage of  $BW_{\text{eff}}$  of 15.5 GHz, ranging from 2.5 to 18 GHz, at a very wide  $d$  range of 1–6 mm. Table I summarizes some important EM absorption properties of some related previous works at the largest reflection loss (i.e., the lowest  $RL$  value) for comparison. Our hybrid composites exhibit improved properties in terms of stronger absorption, broader absorption bandwidth, thinner thickness, and wider thickness range. Thus, the present study provides an effective and alternative way to improve the GHz EM absorption properties.

#### IV. CONCLUSION

We have demonstrated a new approach to improve the EM absorption properties of state-of-the-art core/shell-structured magnetic/dielectric nanocapsules by decorating small Fe/C nanocapsules of  $\sim 4$  nm mean diameter on the surfaces of large Fe<sub>2</sub>B/C nanocapsules of  $\sim 50$  nm mean diameter to form novel Fe/C@Fe<sub>2</sub>B/C hybrids. We have also shown experimentally and numerically an obvious improvement in GHz EM absorption properties inspired by the simultaneously enhanced dielectric and magnetic losses by an increased interfacial polarization at the Fe/C and Fe<sub>2</sub>B/C heterogeneous interfaces and an additional tip effect by the decoration of small Fe/C nanocapsules. As a result, a giant  $RL$  of  $-49.5$  dB at 10.5 GHz and a broad  $BW_{\text{eff}}$  (for  $RL < -10$  dB) of 8 GHz (7.7–15.7 GHz) are achieved at a thin  $d$  of 2.1 mm, together with an extremely broad coverage of  $BW_{\text{eff}}$  of 15.5 GHz (2.5–18 GHz) at a very wide  $d$  range of 1–6 mm. Our work provides a new dimension to realize high-performance EM absorbers in the GHz range.

#### ACKNOWLEDGMENTS

This work was supported by the Research Grants Council of the HKSAR Government (15217917) and The Hong Kong Polytechnic University (G-YBLL and G-YBPP).

#### REFERENCES

- [1] X. Huang, X. Yan, L. Xia, P. Wang, Q. Wang, X. Zhang, B. Zhang, H. Zhao, G. Wen, *Scr. Mater.* 120 (2016) 107.
- [2] X.F. Zhang, Y. Rao, J.J. Guo, G.W. Qin, *Carbon* 96 (2016) 972.
- [3] X.G. Liu, X.L. Li, J.Y. Yu, Y.P. Sun, *Mater. Lett.* 223 (2018) 203.
- [4] L.L. Xiong, M. Yu, J. Liu, S.M. Li, B. Xue, *RSC Adv.* 7 (2017) 14733–14741.
- [5] G.Z. Shen, B.Q. Mei, H.Y. Wu, H.Y. Wei, X.M. Fang, Y.W. Xu, *J. Phys. Chem. C* 121 (2017) 3846–3853.
- [6] F. Qin, H.X. Peng, *Prog. Mater. Sci.* 58 (2013) 183–259.
- [7] X.Q. Shen, F.Z. Song, J. Xiang, M.Q. Liu, Y.W. Zhu, Y.D. Wang, *J. Am. Ceram. Soc.* 95 (2012) 3863.
- [8] X.G. Liu, Y.Y. Wu, X.L. Li, J.Y. Yu, Y.P. Sun, *Ceram. Int.* 44 (2018) 13654.
- [9] H. Wang, Y.Y. Dai, W.J. Gong, D.Y. Geng, S. Ma, D. Li, W. Liu, Z.D. Zhang, *Appl. Phys. Lett.* 102 (2013) 223113.
- [10] F. Qin and C. Brosseau, *J. Appl. Phys.* 111 (2012) 061301.
- [11] Z.B. Guo, H. Huang, D. Xie, H. Xia, *Sci. Rep.* 7 (2017) 11331.
- [12] X.G. Liu, C.Y. Cui, J.Y. Yu, Y.P. Sun, A.L. Xia, *Mater. Lett.* 225 (2018) 1.
- [13] L.W. Jiang, Z.H. Wang, D. Li, D.Y. Geng, Y. Wang, *RSC Adv.* 5 (2015) 40384.
- [14] Y.X. Huang, H.Y. Zhang, G.X. Zeng, Z.H. Li, D.F. Zhang, H.P. Zhu, R.F. Xie, L.M. Zheng, J.H. Zhu, *J. Alloys Compd.* 682 (2016) 138.
- [15] X.G. Liu, J.Y. Yu, C.Y. Cui, Y.P. Sun, X.L. Li, Z.X. Li, *J. Phys. D Appl. Phys.* 51 (2018) 265002.
- [16] L.W. Jiang, Z.H. Wang, D.Y. Geng, Y.M. Lin, Y. Wang, J. An, J. He, D. Li, W. Liu, Z.D. Zhang, *Carbon* 95 (2015) 910.
- [17] X.F. Zhang, P.F. Guan, J.J. Guo, *Part. Part. Syst. Charact.* 30 (2013) 842.
- [18] R.D. Ramdan, T. Takaki, Y. Tomita, *Mater. Trans.* 49 (2008) 2625.
- [19] S. Ma, Y.B. Wang, D.Y. Geng, J. Li, Z.D. Zhang, *J. Appl. Phys.* 98 (2005) 094304.
- [20] M. Mustajic, D. Pajic, N. Novosel, E. Babic, K. Zadro, M. Cindric, *Croat. Chem. Acta* 83 (2010) 275.
- [21] H.L. Lv, H.Q. Zhang, G.B. Ji, Z.C.J. Xu, *ACS Appl. Mater. Interfaces* 8 (2016) 6529.
- [22] X.B. Xie, Y. Pang, H. Kikuchi, T. Liu, *Phys. Chem. Chem. Phys.* 18 (2016) 30507.